

1 **Future Climate Change in the Thermosphere under**
2 **Varying Solar Activity Conditions.**

3 **M. K. Brown^{1,2}, H. G. Lewis², A. J. Kavanagh³, I. Cnossen³, S. Elvidge¹**

4 ¹Space Environment and Radio Engineering Group (SERENE), University of Birmingham

5 ²University of Southampton

6 ³British Antarctic Survey

7 **Key Points:**

- 8 • Scaling factors have been created which allow empirical models to account for fu-
9 ture carbon dioxide induced thermospheric density reductions
10 • The reductions in neutral density have been mapped onto the Shared Socioeco-
11 nomic Pathways to show potential future scenarios
12 • Densities at 400 km are 13 to 30 % lower under high and low solar activity respec-
13 tively in the SSP1-2.6 scenario when CO₂ peaks at 474 ppm

Corresponding author: Matthew K. Brown, m.brown.12@bham.ac.uk

Abstract

Increasing carbon dioxide concentrations in the mesosphere and lower thermosphere are increasing radiative cooling in the upper atmosphere, leading to thermospheric contraction and decreased neutral mass densities at fixed altitudes. Previous studies of the historic neutral density trend have shown a dependence upon solar activity, with larger F10.7 values resulting in lower neutral density reductions. To investigate the impact on the future thermosphere, the Whole Atmosphere Community Climate Model with ionosphere and thermosphere extension (WACCM-X) has been used to simulate the thermosphere under increasing carbon dioxide concentrations and varying solar activity conditions. These neutral density reductions have then been mapped onto the Shared Socioeconomic Pathways (SSPs) published by the Intergovernmental Panel on Climate Change (IPCC). The neutral density reductions can also be used as a scaling factor, allowing commonly used empirical models to account for CO₂ trends. Under the “best case” SSP1-2.6 scenario, neutral densities reductions at 400 km altitude peak (when CO₂ = 474 ppm) at a reduction of 13 to 30% (under high and low solar activity respectively) compared to the year 2000. Higher CO₂ concentrations lead to greater density reductions, with the largest modelled concentration of 890 ppm resulting in a 50 to 77 % reduction at 400 km, under high and low solar activity respectively.

Plain Language Summary

Carbon dioxide (CO₂) concentrations are increasing throughout the atmosphere, not just at ground level. While this results in global warming in the lower atmosphere, the much less dense upper atmosphere does not trap the radiated heat, resulting in cooling of the upper atmosphere. As the upper atmosphere cools, it contracts, reducing the atmospheric density at a fixed altitude. Satellites travelling in low Earth orbit, such as the International Space Station at 400 km altitude, experience atmospheric drag, slowly reducing their altitude until they ‘re-enter’ and burn up in the lower, denser atmosphere. Reducing neutral densities will increase satellite orbital lifetimes as they experience less drag. The upper atmosphere has been simulated under increasing CO₂ concentrations and solar activity conditions. This has also been linked to potential future CO₂ concentration scenarios. Scaling factors have been created allowing simpler, faster models to account for CO₂ density reductions. Under a best-case scenario (SSP1-2.6) where CO₂ concentrations peak in around the year 2065 and then decline, densities at 400 km are 13 to 30% lower compared to the year 2000 at the CO₂ peak concentration, and then recover as CO₂ reduces. However, densities continue to reduce if CO₂ concentrations keep rising.

1 Introduction

Carbon dioxide (CO₂) exists throughout the atmosphere (shown in Figure 1) (Yue et al., 2015) with a roughly constant concentration in the turbulent atmosphere below the homopause (around 90 km altitude). Gravitational separation asymptotically decreases the concentration with altitude trending towards zero in the lower thermosphere (around 200 km).

Carbon dioxide can gain energy via collisions with molecules or ions in the atmosphere, or absorbing infra-red (IR) radiation. It can then lose that energy via collisions, or emission of IR radiation (at 15 μm). In the dense lower atmosphere, collisions dominate, and any emitted IR radiation has a short mean free path, being quickly recaptured and trapping heat locally, leading to the greenhouse effect. In the less-dense upper atmosphere, collisions are much less frequent, so CO₂ is more likely to lose energy via IR emission, which has a much longer mean free path, allowing heat to escape the locale, cooling the upper atmosphere. As the upper atmosphere cools, it contracts, resulting in the neutral density reducing at a given fixed altitude.

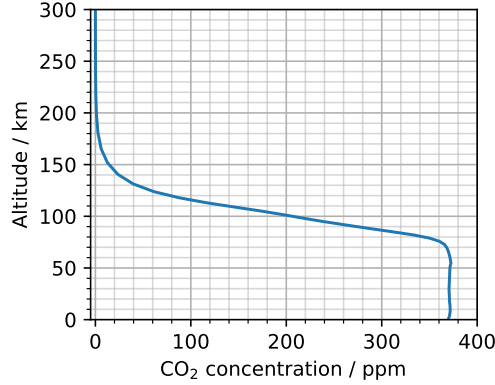


Figure 1. Altitude profile of carbon dioxide concentration, from ground-level through to the lower thermosphere. This example is a global average of WACCM-X output for the year 2000.

64 Similarly to CO_2 , Nitric oxide (NO) also cools the upper atmosphere with IR emis-
 65 sion at $5.3 \mu\text{m}$. Concentrations of NO , and also atomic oxygen (O), vary with solar acti-
 66 vity levels (Mlynczak et al., 2014). This changes the ratio of NO to CO_2 , as well as the
 67 temperature and collision rates with O , such that the magnitude of neutral density re-
 68 ductions in the upper atmosphere is dependent on solar activity. The largest reductions
 69 are seen under low solar activity, when CO_2 is relatively more important for the ther-
 70 mosphere’s energy budget. The large amount of molecular nitrogen (N_2) in the lower at-
 71 mosphere acts as a reservoir, such that additional nitrogen dioxide (NO_2) released as a
 72 greenhouse gas is assumed to have minimal impact on NO concentrations.

73 A large number of previous studies have both modelled and observed the reduc-
 74 ing density trend first predicted by Roble and Dickinson (1989). Observed neutral den-
 75 sity reductions are summarized in Table 1, modelled values in Table 2, and Figure 2 shows
 76 the altitude profile of both observed and modelled reductions in literature. All values
 77 have been standardized to a density trend given in ‘% per decade’. While the magnitude
 78 of the reductions vary across the literature, all studies agree on a reducing density trend
 79 within the upper atmosphere. The studies that also binned density trends by solar ac-
 80 tivity agreed that the trend is larger in magnitude under low solar activity.

81 These secular trends in neutral density have an impact on the space debris envi-
 82 ronment in low Earth orbit (LEO), reducing atmospheric drag acting on orbiting objects
 83 and increasing their orbital lifetimes (Lewis et al., 2011). Models of the space debris en-
 84 vironment make use of computationally fast empirical atmospheric models to propagate
 85 space debris while accounting for atmospheric drag, however these empirical atmospheric
 86 models do not account for secular CO_2 trends. The aims of this study are therefore twofold.
 87 Firstly to understand how the magnitude of neutral density reductions with increasing
 88 CO_2 concentration varies with solar activity, and secondly to provide scaling factors which
 89 allow empirical atmospheric models to account for long-term trends caused by CO_2 emis-
 90 sions. These scaling factors maintain the speed and ease-to-run advantages of empiri-
 91 cal models over numerical models, while allowing for CO_2 induced trends to be included
 92 in orbital lifetime estimation and debris environment modelling.

93 2 Model

94 The Whole Atmosphere Community Climate Model with thermosphere and iono-
 95 sphere extension (WACCM-X) was used to model the thermospheric response to increas-

Table 1. Summary of observed (derived) neutral density trends at 400 km altitude. “Model used” refers to the atmospheric model used to remove the dominant solar cycle variation, and detrend the data.

Study	Model Used	F10.7 (sfu)	Period	Density Trend (% per decade)
Keating et al. (2000) ^a	MET99	~75	1976, 1986, 1996	-4.9 ± 1.3
Emmert et al. (2004)	NRLMSISE-00	<90	1996 - 2001	-3.8
Emmert et al. (2004)	NRLMSISE-00	All	1996 - 2001	-2.8 ± 1.0
Marcos et al. (2005)	NRLMSISE-00	All	1970 - 2000	-1.7 ± 0.2
Emmert et al. (2008)	GAMDM	<75	1967 - 2007	-5.5 ± 1.4
Emmert et al. (2008)	GAMDM	170 to 220	1967 - 2007	-2.1 ± 0.9
Saunders et al. (2011)	NRLMSISE-00	<90	1970 - 2010	-7.2
Saunders et al. (2011)	NRLMSISE-00	All	1970 - 2010	-5.4 ± 3
Saunders et al. (2011)	NRLMSISE-00	>90	1970 - 2010	-4.0
Emmert and Picone (2011)	GAMDM	All	1967 - 2005	-1.94 ± 0.68
Emmert (2015)	GAMDM2.1	60 to 75	1967 - 2005	-3.1 ± 1.6
Emmert (2015)	GAMDM2.1	60 to 75	1967 - 2013	-7.2 ± 1.2
Emmert (2015)	GAMDM2.1	180 to 500	1967 - 2005	-3.0 ± 0.7
Emmert (2015)	GAMDM2.1	180 to 500	1967 - 2013	-3.0 ± 0.8
Weng et al. (2020)	ANNM	All	1967 - 2013	-1.7

^a 350 km altitude**Table 2.** Summary of the modelled historic neutral density trends at 400 km altitude.

Study	Model Used	F10.7 (sfu)	Period	Density Trend (% per decade)
Qian et al. (2006)	TIME-GCM (1D)	70	1970 - 2000	-2.5 ^a
Qian et al. (2006) ^b	TIME-GCM (1D)	All	1970 - 2000	-1.7
Qian et al. (2006)	TIME-GCM (1D)	210	1970 - 2000	-0.75 ^a
Solomon et al. (2015)	TIME-GCM	70	1996 - 2008	-4.9 or -6.8 ^c
Solomon et al. (2015)	TIME-GCM	200	1996 - 2008	-1.8 or -2.1 ^c
Solomon et al. (2018)	WACCM-X	70	1974 - 2003	-3.9
Solomon et al. (2019)	WACCM-X	200	1974 - 2003	-1.7
Cnossen (2020)	WACCM-X 2.0	All	1950 - 2015	-2.8 ± 0.6
Brown et al. (2021)	WACCM-X	70	1975 - 2005	-5.8

^a Average of the 350 km and 450 km values^b Result was re-presented by (Qian & Solomon, 2011)^c k_q , CO₂-O collisional deactivation rate, of 1.5×10^{-12} or $3.0 \times 10^{-12} \text{ cm}^3 \text{ s}^{-1}$

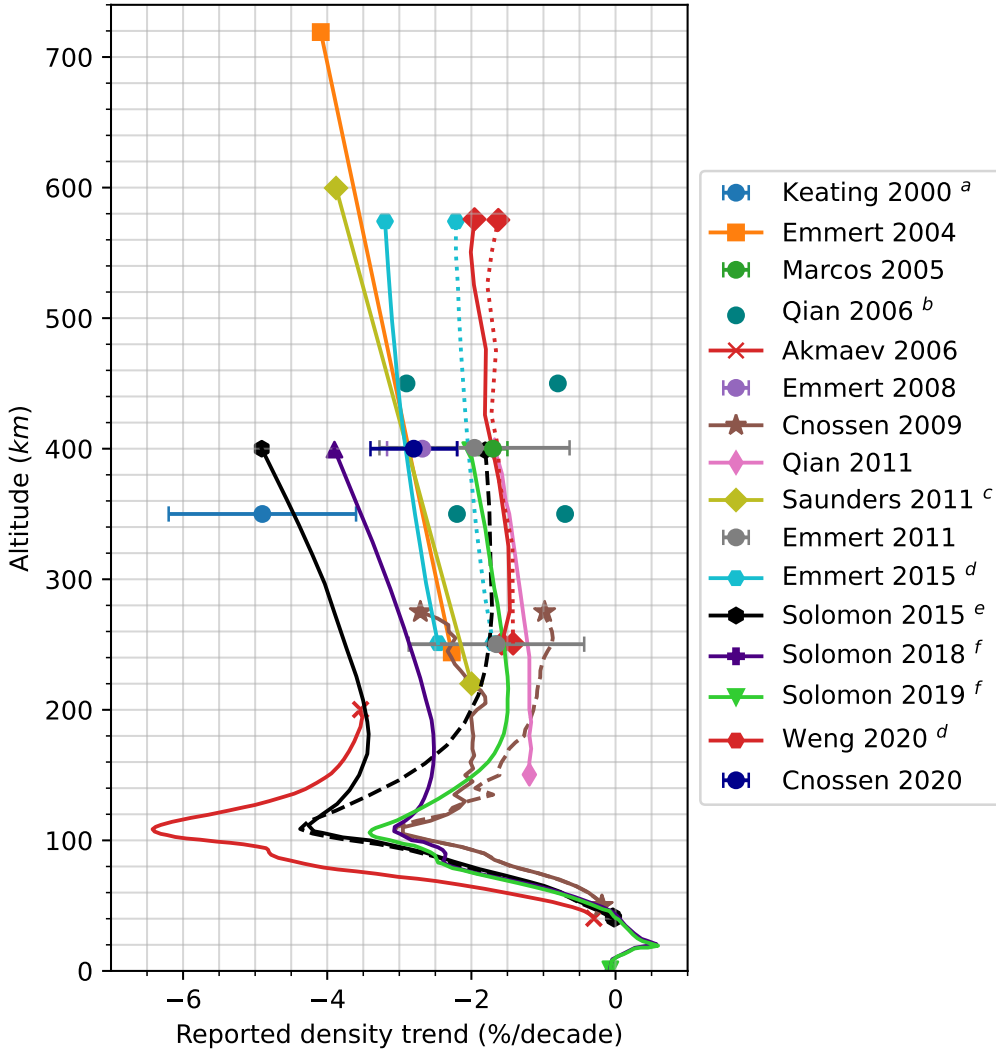


Figure 2. Summary of historical density trends at 400 km in the literature for varying solar activity levels, with detail on values used given in Tables 1 and 2. Error bars are provided where available. Updated version of similar figures in Emmert et al. (2008) and Solomon et al. (2015).

^a Keating et al. (2000) value at 350 km.

^b Plotted line is mean of 350 and 450 km trends in Qian et al. (2006).

^c Saunders et al. (2011) used large binning for F10.7, so the lines denote trends found for F10.7 less than or greater than 90 sfu.

^d Emmert (2015) and Weng et al. (2020) calculated the trend over different periods. The solid line denotes 1967 to 2005 and the dotted line denotes 1967 to 2013.

^e CO₂-O quenching rate, k_q , affects the CO₂ cooling rate and therefore the magnitude of trend. Solomon et al. (2015) used the default k_q of the model, 1.5×10^{-12} (solid line), and also 3.0×10^{-12} (dashed line).

^f Solomon et al. (2018) and Solomon et al. (2019) use the same methodology, but at low and high solar activity values respectively.

ing levels of CO₂, with the model fully described by Liu et al. (2010). The model is part of the Community Earth System Model (CESM) (Hurrell et al., 2013), maintained by the National Center for Atmospheric Research (NCAR). Version 1.2.2 of the model was used rather than the newer 2.0 (Liu et al., 2018) to build upon the reprocessed results of Brown et al. (2021) and allow for direct comparison. As a whole atmosphere numerical model, WACCM-X solves for the physics, chemistry and dynamics of the atmosphere, starting from some initial state and moving forwards in time. This allows ground-level CO₂ to propagate upwards to the thermosphere. A 1.9 by 2.5 degree latitude by longitude grid with quarter scale height vertical resolution was used up to a maximum model height of 4×10^{-10} hPa. This top level of the model varies in altitude between around 350 to 600 km depending upon energy input.

3 Methodology

WACCM-X has been used to simulate the whole atmosphere under different, fixed carbon dioxide concentrations, under low and high solar activity conditions, as well as varying solar activity conditions at one fixed, high CO₂ concentration. As a numerical model, WACCM-X requires a spin-up time for the model to move from its initial conditions towards a steady state more representative of the input conditions. A sudden, large increase in ground-level CO₂ takes a substantial amount of time to propagate through to the upper atmosphere. To speed up the spin-up process, the CO₂ profile in the initial state of the year 2000 (Figure 1) is scaled by the relative increase in ground-level CO₂ concentration. Above 60 km, photodissociation breaks CO₂ into carbon monoxide (CO) and O, which can then reform, such that CO₂ and CO exist in chemical equilibrium in the thermosphere. Therefore the CO profile is scaled similarly to CO₂. After this scaling, WACCM-X has 4 months of spin-up before data is used for analysis, allowing for a steady state to be reached.

Geomagnetic activity was held at a Kp value of 0 throughout the simulations to remove geomagnetic activity effects, and to match results with Brown et al. (2021). It is noted that the most commonly occurring Kp value is 1, and may have been a better choice as the default. However, Emmert (2015) identified no significant difference between these two values in historic observed trends.

With increasing traffic to LEO orbits, there is a strong need to understand the neutral density trends in this region. The US Naval Research Laboratory’s Mass Spectrometer and Incoherent Scatter radar model (NRLMSISE-00) (Picone et al., 2002) shows that helium can contribute over 15% of the total, globally averaged neutral density at altitudes higher than around 500 km during low solar activity, but helium is not modelled by WACCM-X. The neutral density extrapolation technique used in Brown et al. (2021) failed to account for helium, so extrapolation and neutral density trends were limited in altitude to 500 km. In this study, a different extrapolation technique which includes helium is used instead (which is also applied to the Brown et al. (2021) results). As helium is chemically inert, it can be added by an uncoupled model (Kim et al., 2012; Sutton et al., 2015). In post-processing, NRLMSISE-00 is used to calculate atomic oxygen and helium number densities under similar solar activity, times, and grid points as the WACCM-X simulations. These NRLMSISE-00 helium profiles are then scaled by the atomic oxygen fractional difference between the NRLMSISE-00 and WACCM-X profiles, as in:

$$\text{He}_{\text{WACCM-X}} = \frac{\text{O}_{\text{WACCM-X}}}{\text{O}_{\text{NRLMSISE-00}}} \text{He}_{\text{NRLMSISE-00}} \quad (1)$$

at each grid point. The number density profile of each species is then extrapolated to higher altitudes using Bates-Walker (Walker, 1965) profiles via

$$n(i|z) = n(i|\infty) \exp \left[- \frac{m_i g_{ref}}{kT_\infty} \frac{(z - z_\infty)(R + z_{ref})}{R + z} \right] \quad (2)$$

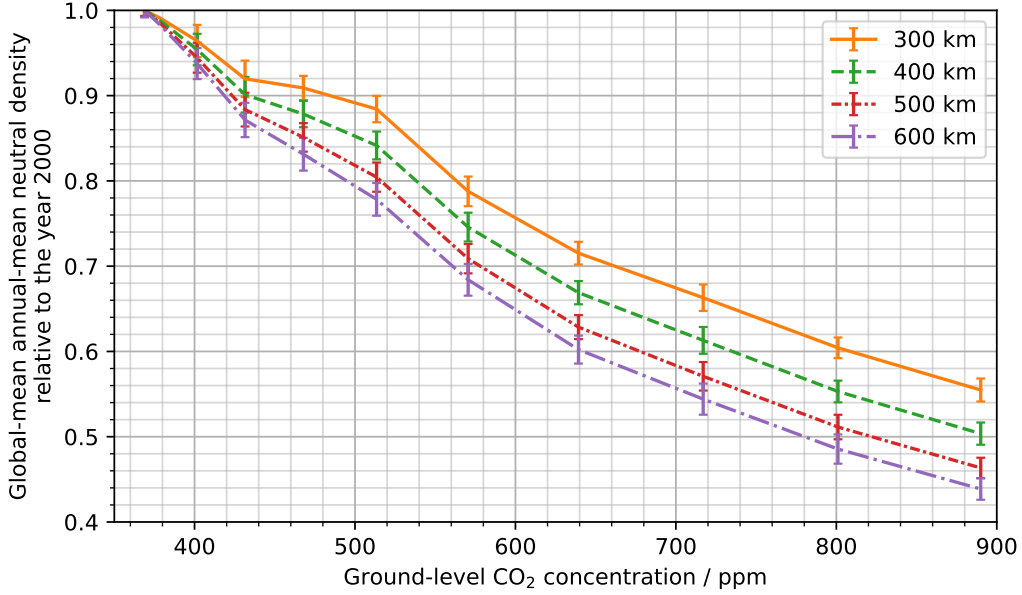


Figure 3. Neutral density reductions relative to the year 2000, at F10.7 of 200 sfu, under increasing ground-level carbon dioxide concentrations. These can be used as scaling factors for an empirical thermospheric model to include CO₂ density reductions, under high solar activity conditions.

142 where $n(i|z)$ is the number density of constituent i at altitude z , m_i is the mass of the
 143 constituent, g_{ref} is the gravity at the reference altitude z_{ref} (taken as the level below
 144 the top level of WACCM-X), k is the Boltzmann constant and R is the Earth's radius.
 145 T_∞ is the exospheric temperature, which is assumed to be the WACCM-X top level tem-
 146 perature. z_∞ is the altitude at which the exospheric temperature is taken. The number
 147 density profiles are converted to mass densities, and neutral mass density is then obtained
 148 by summing the O and He profiles.

149 4 High Solar Activity Results

150 WACCM-X was used to simulate carbon dioxide concentrations which correspond
 151 to Representative Concentration Pathway 8.5 (RCP8.5) (Intergovernmental Panel on Cli-
 152 mate Change (IPCC), 2014) for 2015 to 2095 inclusive in 10 year steps, as well as the
 153 year 2000 as a reference point. These concentrations were chosen to match (Brown et
 154 al., 2021), but 2005 was neglected due to the small change expected with respect to the
 155 year 2000. Each of these was run cyclically for five years and the global-mean annual-
 156 means taken, where five years was chosen to better understand the standard deviation
 157 between different model realizations. Results are shown in Figure 3. Global-mean annual-
 158 means are taken to remove seasonal dependencies.

159 5 Varying Solar Activity Results

160 Historic studies, and the above results (compared against the low solar activity re-
 161 sults of Brown et al. (2021)), show that neutral density reductions are smaller in mag-
 162 nitude during high solar activity. To understand how the reduction depends on solar ac-
 163 tivity conditions in more detail, WACCM-X was used to simulate the years 2000 and 2065

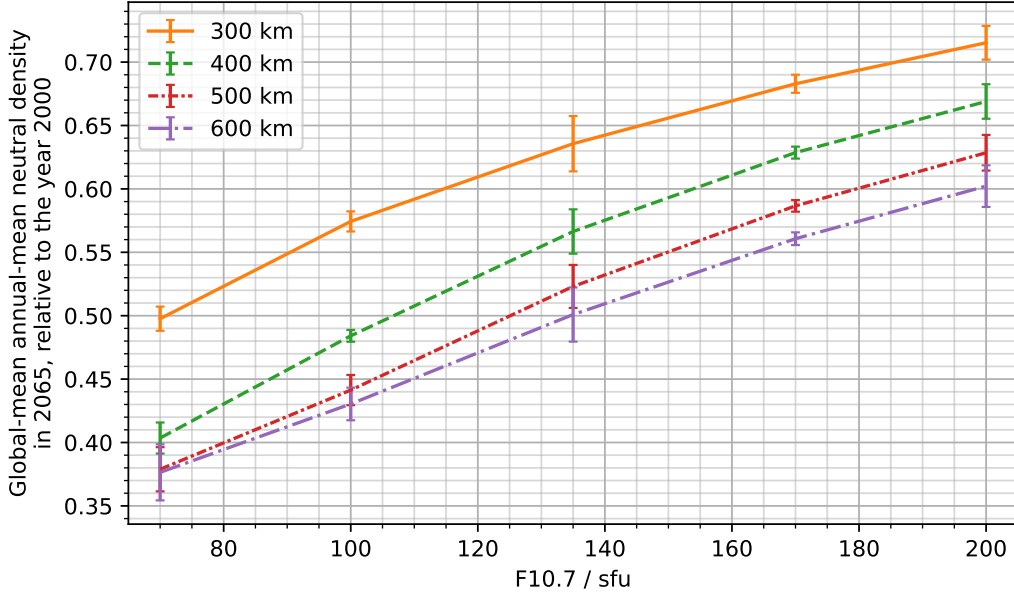


Figure 4. Neutral density reductions relative to the year 2000, at a CO₂ concentration of 639 ppm, under varying solar activity conditions.

164 (639 ppm) under F10.7 values of 100, 135, and 170 sfu. This provided enough points to
 165 outline the relationship (linear vs nonlinear) with the limited computing resources avail-
 166 able. The year 2065 (639 ppm) was chosen as a large enough CO₂ concentration to re-
 167 sult in larger neutral density reductions to identify the trend, while being low enough
 168 that it appears in most RCP and Shared Socioeconomic Pathway (SSP) scenarios. Each
 169 of these was run cyclically for 2 years and the global-mean annual-means taken, where
 170 2 years was chosen due to computing time limitations. Results are shown in Figure 4,
 171 along with the equivalent 70 sfu values from the reprocessed results of Brown et al. (2021)
 172 using the updated methodology, and 200 sfu of Figure 3.

173 To combine the low, high and varying solar activity results, Figure 5 uses 2D cubic
 174 interpolation on each altitude shell to obtain the F10.7-CO₂ combinations which were
 175 not simulated with WACCM-X. This inherently assumes the relationship shown in Fig-
 176 ure 4 maps to other CO₂ concentrations, and is scaled to the lower and upper limits of
 177 the low and high solar activity runs. This provides scaling factors relative to the year
 178 2000, dependent upon solar activity (70 to 200 sfu), altitude (200 to 1000 km), and CO₂
 179 concentrations (around 370 to 890 ppm).

180 6 Discussion

181 In both the low solar activity results of Brown et al. (2021) and the high solar ac-
 182 tivity results of Figure 3, there is a sudden decrease in the rate at which neutral den-
 183 sities reduce between CO₂ concentrations of around 440 and 520 ppm, which then re-
 184 covers by 550 ppm. This does not correlate with any of the input parameters to WACCM-
 185 X, so it cannot be readily attributed to it being an artifact of the model itself, a com-
 186 bination of input parameters, or an unidentified physical phenomenon.

187 While the historic trends summarized in Figure 2 often present results in units of
 188 “% per decade”, this inherently includes the historic increase in carbon dioxide. Extrap-
 189 olating “% per decade” trends forward assumes the rate of increase in CO₂ concentra-

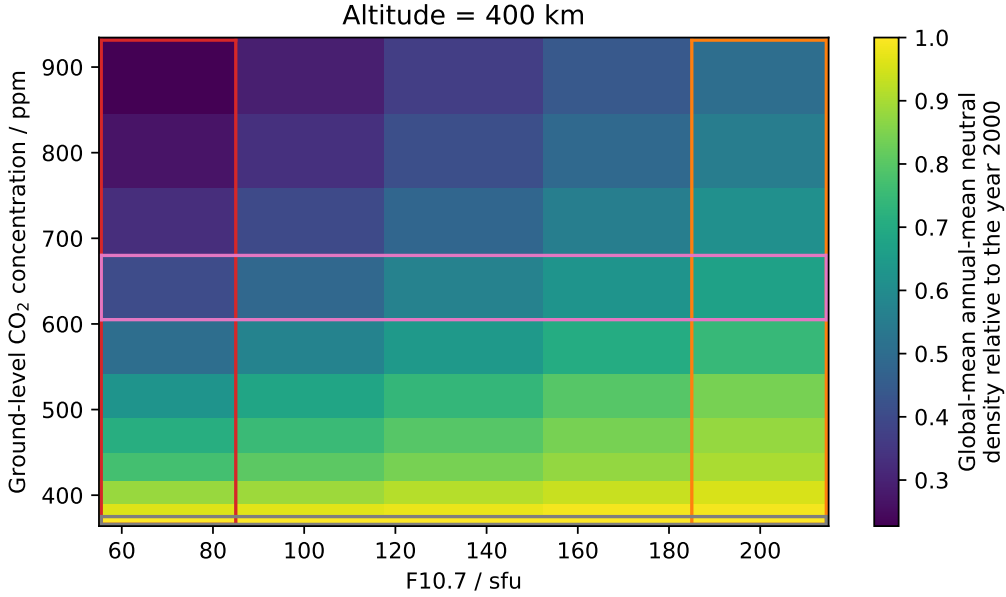


Figure 5. Neutral density reductions at 400 km altitude. Bins outlined in red indicate low F10.7 runs at 70 sfu (reprocessed from Brown et al. (2021)), orange are high F10.7 (200 sfu of Figure 3), pink are varying F10.7 runs at a fixed 639 ppm (shown in Figure 4), and grey is the reference line (year 2000) where all ratios equal 1. Other bins are obtained by 2D cubic interpolation.

190 tions will remain constant. The Intergovernmental Panel on Climate Change (IPCC) has
 191 published the Shared Socioeconomic Pathways (SSPs) which contain future possible CO₂
 192 concentrations (Lee et al., 2023). These reduce the extensive possibilities in the litera-
 193 ture to a limited number of scenarios which can be commonly used between studies. The
 194 four most similar to the older RCPs are shown in Figure 6.

195 The results of Figure 5, can then be mapped to each SSP’s future CO₂ concentra-
 196 tions, as shown in Figure 7. It has been shown that solar activity has a substantial im-
 197 pact on neutral density reductions, but solar activity forecasts on the order of years to
 198 decades are notoriously difficult (Nandy, 2021). Therefore to demonstrate the solar ac-
 199 tivity impact, solar cycles 23 and 24 are repeated. These density reductions are applied
 200 in addition to the order-of-magnitude change in neutral density caused by solar activ-
 201 ity, and can be applied to output from empirical models (by assuming that model is an
 202 accurate representation of the year 2000). In the SSP1-2.6 scenario, as CO₂ concentra-
 203 tions peak and decline, neutral densities begin to recover. However, looking at this “best-
 204 case” scenario, the reduced neutral densities are between 13 to 30% lower during the peak
 205 CO₂ period, which will substantially increase orbital lifetimes. In general, this will in-
 206 crease the likelihood of collision during an object’s lifetime, creating more fragments, which
 207 further increases the likelihood of collision in a feedback loop. This is being investigated
 208 in further work.

209 7 Conclusions

210 WACCM-X has been used to simulate the thermospheric response and contraction
 211 to increasing CO₂ concentrations under varying solar activity conditions. In general, the
 212 neutral density reductions increase in magnitude with altitude, increase with carbon diox-

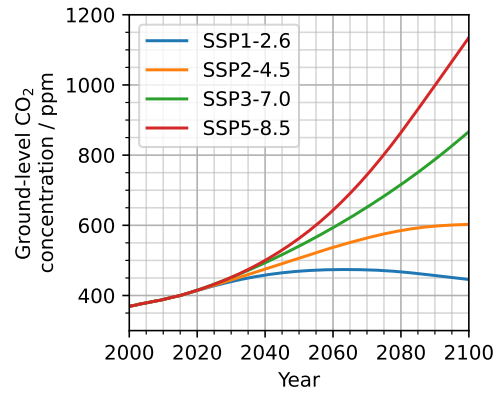


Figure 6. Future carbon dioxide concentration taken from four of the Shared Socioeconomic Pathways (SSPs) published by the IPCC (Lee et al., 2023).

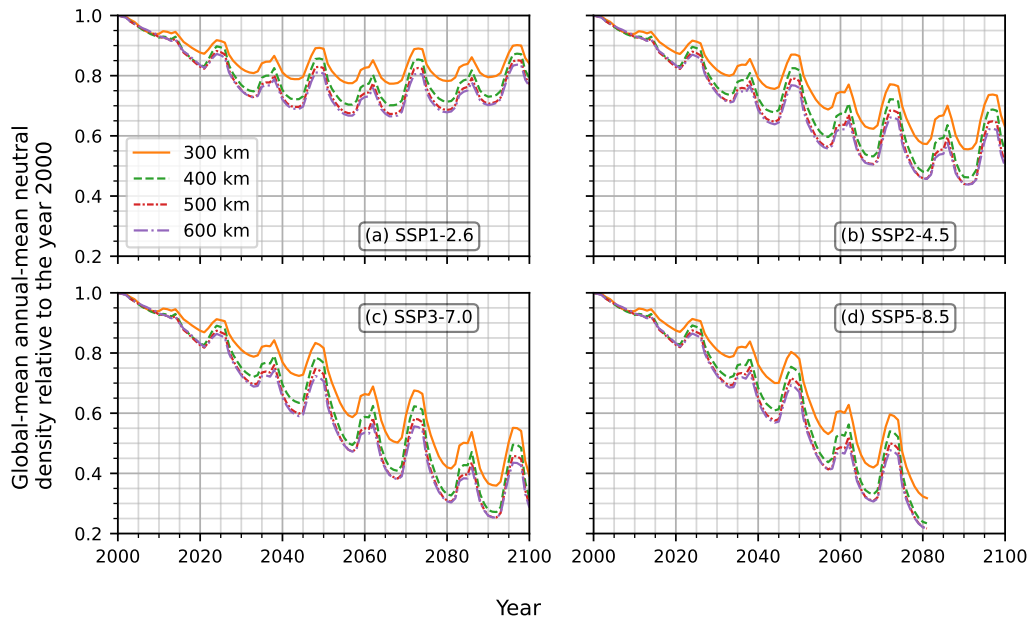


Figure 7. Density reductions under the four SSPs shown in Figure 6. Solar cycles 23 and 24 are repeated into the future to demonstrate the impact of solar activity on these impacts. Subfigure d, showing SSP5-8.5, ends in 2080 as higher CO₂ values were not modelled.

213 ide concentration, and decrease with solar activity (F10.7). Through use of the future
 214 CO₂ concentration scenarios of the SSPs, neutral density reductions can be mapped onto
 215 years. These scaling factors are being made available as a method of including carbon
 216 dioxide-induced neutral density reductions in empirical models, as a much faster solu-
 217 tion compared to numerical models. This requires assuming the empirical model, is an
 218 accurate representation of the year 2000. However, this opens up including long-term
 219 trends into applications such as orbital propagation, lifetime estimation, or space debris
 220 environment evolution, and without the need to fully replace the currently used atmo-
 221 spheric models.

222 8 Open Research

223 The authors acknowledge the contributions of those who helped develop CESM and
 224 WACCM-X. These models are publicly available from <http://www.cesm.ucar.edu/models/>.
 225 The data produced and processed for this study is available at:
 226 <https://doi.org/10.5285/09198c58032d4b8197fd7c6748b92785>

227 The scaling factors allowing empirical models to account for CO₂ reductions are
 228 available at:
 229 <https://doi.org/10.25500/edata.bham.00001075>

230 Acknowledgments

231 The authors acknowledge the use of the IRIDIS High Performance Computing Fa-
 232 cility, and associated support services at the University of Southampton, in the comple-
 233 tion of this work. This research was supported by the International Space Science In-
 234 stitute (ISSI) in Bern, through ISSI International Team project #544 (Impacts of Cli-
 235 mate Change on the Middle and Upper Atmosphere and Atmospheric Drag of Space Ob-
 236 jects). M. K. Brown and S. Elvidge are supported by the UK Space Weather Instrumen-
 237 tation, Measurement, Modelling and Risk (SWIMMR) Programme, National Environ-
 238 mental Research Council (NERC) Grants NE/V002643/1 and NE/V002708/1. I. Cnossen
 239 was supported by a Natural Environment Research Council (NERC) Independent Re-
 240 search Fellowship (NE/R015651/1). A. J. Kavanagh was supported by the British Antarc-
 241 tic Survey Polar Science for Planet Earth Programme, funded by NERC as part of the
 242 UKRI.

243 References

- 244 Brown, M. K., Lewis, H. G., Kavanagh, A. J., & Cnossen, I. (2021). Future de-
 245 creases in thermospheric neutral density in low Earth orbit due to carbon
 246 dioxide emissions. *Journal of Geophysical Research: Atmospheres*, *126*(8),
 247 1–11. doi: <https://doi.org/10.1029/2021JD034589>
- 248 Cnossen, I. (2020). Analysis and attribution of climate change in the upper at-
 249 mosphere from 1950 to 2015 simulated by WACCM-X. *Journal of Geophysical*
 250 *Research: Space Physics*, *125*, e2020JA028623. doi: <https://doi.org/10.1029/2020JA028623>
- 251 Emmert, J. T. (2015). Altitude and solar activity dependence of 1967–2005 ther-
 252 mospheric density trends derived from orbital drag. *Journal of Geophysical*
 253 *Research: Space Physics*, *120*, 2940–2950. doi: <https://doi.org/10.1002/2015JA021047>
- 254 Emmert, J. T., & Picone, J. M. (2011). Statistical uncertainty of 1967–2005 ther-
 255 mospheric density trends derived from orbital drag. *Journal of Geophysical Re-*
 256 *search: Space Physics*, *116*. doi: <https://doi.org/10.1029/2010JA016382>
- 257 Emmert, J. T., Picone, J. M., Lean, J. L., & Knowles, S. H. (2004). Global
 258 change in the thermosphere: Compelling evidence of a secular decrease
 259
 260

- 261 in density. *Journal of Geophysical Research: Space Physics*, 109. doi:
 262 <https://doi.org/10.1029/2003JA010176>
- 263 Emmert, J. T., Picone, J. M., & Meier, R. R. (2008). Thermospheric global average
 264 density trends, 1967-2007, derived from orbits of 5000 near-Earth objects. *Geo-*
 265 *physical Research Letters*, 35. doi: <https://doi.org/10.1029/2007GL032809>
- 266 Hurrell, J. W., Holland, M. M., Gent, P. R., Ghan, S., Kay, J. E., J., K. P., et al.
 267 (2013). The Community Earth System Model: A framework for collaborative
 268 research. *Bulletin of the American Meteorological Society*, 94(9), 1339–1360.
 269 doi: <https://doi.org/10.1175/BAMS-D-12-00121.1>
- 270 Intergovernmental Panel on Climate Change (IPCC). (2014). *Climate change 2013*
 271 *– the physical science basis: Working group I contribution to the Fifth Assess-*
 272 *ment Report of the Intergovernmental Panel on Climate Change*. Cambridge
 273 University Press. doi: <https://doi.org/10.1017/CBO9781107415324>
- 274 Keating, G. M., Tolson, R. H., & Bradford, M. S. (2000). Evidence of long term
 275 global decline in the Earth’s thermospheric densities apparently related to
 276 anthropogenic effects. *Geophysical Research Letters*, 27(10), 1523–1526. doi:
 277 <https://doi.org/10.1029/2000GL003771>
- 278 Kim, J. S., Urbina, J. V., Kane, T. J., & Spencer, D. B. (2012). Improvement of
 279 TIE-GCM thermospheric density predictions via incorporation of helium data
 280 from NRLMSISE-00. *Journal of Atmospheric and Solar-Terrestrial Physics*,
 281 77, 19-25. doi: <https://doi.org/10.1016/j.jastp.2011.10.018>
- 282 Lee, H., Calvin, K., Dasgupta, D., Krinmer, G., Mukherji, A., Thorne, P., ... others
 283 (2023). Synthesis report of the IPCC Sixth Assessment Report (AR6), Longer
 284 report. IPCC.
- 285 Lewis, H. G., Saunders, A., Swinerd, G. G., & Newland, R. J. (2011). Effect of
 286 thermospheric contraction on remediation of the near-Earth space debris
 287 environment. *Journal of Geophysical Research: Space Physics*, 116. doi:
 288 <https://doi.org/10.1029/2011JA016482>
- 289 Liu, H. L., Bardeen, C. G., Foster, B. T., Lauritzen, P., Liu, J., Lu, G., ... Wang,
 290 W. (2018). Development and Validation of the Whole Atmosphere Community
 291 Climate Model With Thermosphere and Ionosphere Extension (WACCM-X
 292 2.0). *Journal of Advances in Modeling Earth Systems*, 10(2), 381–402. doi:
 293 <https://doi.org/10.1002/2017MS001232>
- 294 Liu, H. L., Foster, B. T., Hagan, M. E., McInerney, J. M., Maute, A., Qian, L., ...
 295 Oberheide, J. (2010). Thermosphere extension of the Whole Atmosphere
 296 Community Climate Model. *Journal of Geophysical Research: Space Physics*,
 297 115(A12). doi: <https://doi.org/10.1029/2010JA015586>
- 298 Marcos, F. A., Wise, J. O., Kendra, M. J., Grossbard, N. J., & Bowman, B. R.
 299 (2005). Detection of a long-term decrease in thermospheric neutral den-
 300 sity. *Geophysical Research Letters*, 32(4). doi: <https://doi.org/10.1029/2004GL021269>
- 301
- 302 Mlynczak, M. G., Hunt, L. A., Mertens, C. J., Thomas Marshall, B., Russell III,
 303 J. M., Woods, T., ... Gordley, L. L. (2014). Influence of solar variability on
 304 the infrared radiative cooling of the thermosphere from 2002 to 2014. *Geo-*
 305 *physical Research Letters*, 41(7), 2508-2513. doi: <https://doi.org/10.1002/2014GL059556>
- 306
- 307 Nandy, D. (2021). Progress in solar cycle predictions: Sunspot cycles 24–25 in per-
 308 spective: Invited review. *Solar Physics*, 296(3), 54. doi: <https://doi.org/10.1007/s11207-021-01797-2>
- 309
- 310 Picone, J. M., Hedin, A. E., Drob, D. P., & Aikin, A. C. (2002). NRLMSISE-
 311 00 empirical model of the atmosphere: Statistical comparisons and scientific
 312 issues. *Journal of Geophysical Research: Space Physics*, 107(A12). doi:
 313 <https://doi.org/10.1029/2002JA009430>
- 314 Qian, L., Roble, R. G., Solomon, S. C., & Kane, T. J. (2006). Calculated and
 315 observed climate change in the thermosphere, and a prediction for solar cy-

- 316 cle 24. *Geophysical Research Letters*, 33(23). doi: <https://doi.org/10.1029/2006GL027185>
- 317
- 318 Qian, L., & Solomon, S. C. (2011). Thermospheric density: An overview of tempo-
319 ral and spatial variations. *Space Science Reviews*, 168, 147–173. doi: <https://doi.org/10.1007/s11214-011-9810-z>
- 320
- 321 Roble, R. G., & Dickinson, R. E. (1989). How will changes in carbon dioxide and
322 methane modify the mean structure of the mesosphere and thermosphere?
323 *Geophysical Research Letters*, 16(12), 1441–1444. doi: <https://doi.org/10.1029/GL016i012p01441>
- 324
- 325 Saunders, A., Lewis, H. G., & Swinerd, G. G. (2011). Further evidence of long-term
326 thermospheric density change using a new method of satellite ballistic coeffi-
327 cient estimation. *Journal of Geophysical Research: Space Physics*, 116(A2).
328 doi: <https://doi.org/10.1029/2010JA016358>
- 329 Solomon, S. C., Liu, H. L., Marsh, D. R., McInerney, J. M., Qian, L., & Vitt, F. M.
330 (2018). Whole atmosphere simulation of anthropogenic climate change.
331 *Geophysical Research Letters*, 45, 1567–1576. doi: <https://doi.org/10.1002/2017GL076950>
- 332
- 333 Solomon, S. C., Liu, H. L., Marsh, D. R., McInerney, J. M., Qian, L., & Vitt, F. M.
334 (2019). Whole atmosphere climate change : Dependence on solar activi-
335 ty. *Journal of Geophysical Research : Space Physics*, 124, 3799–3809. doi:
336 <https://doi.org/10.1029/2019JA026678>
- 337 Solomon, S. C., Qian, L., & Roble, R. G. (2015). New 3-D simulations of climate
338 change in the thermosphere. *Journal of Geophysical Research: Space Physics*,
339 120, 2183–2193. doi: <https://doi.org/10.1002/2014JA020886>
- 340 Sutton, E. K., Thayer, J. P., Wang, W., Solomon, S. C., Liu, X., & Foster, B. T.
341 (2015). A self-consistent model of helium in the thermosphere. *Jour-
342 nal of Geophysical Research A: Space Physics*, 120(8), 6884–6900. doi:
343 [10.1002/2015JA021223](https://doi.org/10.1002/2015JA021223)
- 344 Walker, J. C. G. (1965). Analytic representation of upper atmosphere densities
345 based on Jacchia’s static diffusion models. *Journal of Atmospheric Sciences*,
346 22, 462–463. doi: [https://doi.org/10.1175/1520-0469\(1965\)022%3C0462:
347 AROUAD%3E2.0.CO;2](https://doi.org/10.1175/1520-0469(1965)022%3C0462:AROUAD%3E2.0.CO;2)
- 348 Weng, L., Lei, J., Zhong, J., Dou, X., & Fang, H. (2020). A machine-learning
349 approach to derive long-term trends of thermospheric density. *Geophysi-
350 cal Research Letters*, 47(6), e2020GL087140. doi: <https://doi.org/10.1029/2020GL087140>
- 351
- 352 Yue, J., Russell III, J., Jian, Y., Rezac, L., Garcia, R., López-Puertas, M., &
353 Mlynczak, M. G. (2015). Increasing carbon dioxide concentration in the
354 upper atmosphere observed by saber. *Geophysical Research Letters*, 42(17),
355 7194–7199. doi: <https://doi.org/10.1002/2015GL064696>